Effect of InSn additives on the structure and tribological characteristics of TiAlZrN nanocomposite coatings on AISI 304 steel

A. A. Lozovan, *Dr. Eng., Prof.* [1]*;*
S. V. Savushikna, *Dr. Eng., Prof.* [1]*, e-mail: sveta_049@mail.ru;*
S. Ya. Betsofen, *Dr. Eng., Prof.* [1]*;*
I. A. Nikolaev, *Cand. Eng., Associate Prof.* [1]

[1] *Moscow Aviation Institute (National Research University), Moscow, Russia*

Solid lubricant coatings based on complex nitride matrices TiAlZrN with InSn additives were obtained on steel AISI 304 by reactive magnetron sputtering. Depending on the indium and TiN content, the structure, phase composition, microhardness and tribological characteristics were studied at room temperature and as a result of stepwise heating of the substrate-film system under fretting wear conditions in contact with a counterbody made of ShKh-15 steel. The surface structure of the coatings changed from homogeneous to finely crystalline with an increase in the indium content from 1.4 to 1.9 at.%, and to microglobular with an increase in the indium content to 5.7 at.%, which was also accompanied by an increase in surface roughness. Indium reflexes are absent in XRD patterns when its content in the coatings is less than 2.6 at.%. The friction coefficients of coatings with different indium contents at room temperature varied from 0.20 to 0.42. The coatings exhibited predominant abrasive and adhesive wear mechanisms. Stepwise heating to 100 and 200°C resulted in a decrease in the friction coefficient to 0.08 and a wear of the nanocrystalline coating containing 1.9 at.% In and 0.2 at.% Sn.

Key words: AISI 304 steel, solid lubricant coating, structure, nanocomposite coating, reactive magnetron sputtering, friction coefficient, hardness, wear.
DOI: 10.17580/cisisr.2026.01.13

Introduction

Austenitic stainless steels are often used in applications requiring high corrosion resistance. However, due to low hardness and wear resistance, their application is limited. Surface modification or the application of a solid lubricant coating (SLC) with increased wear resistance may be a solution to this problem. Nitride and carbonitride-based coatings are often considered as solid lubricant coatings to improve the tribological properties of steel surfaces [1–5]. For example, in [6], the treatment of AISI M2 high-speed steel with various nitride-based coatings, including titanium nitride (TiN), was studied to improve its wear resistance. The TiN coating obtained by reactive plasma spraying on carbon steel, showed superior wear resistance compared to AISI M2 high-speed steel under dry conditions in work [7]. Other commonly used binary nitride coatings, such as CrN and ZrN, have also demonstrated significant potential for extending the service life of metals and tools [8–9].

However, no solid lubricant coating has yet been developed that provides the required friction and wear characteristics for steel surfaces under a wide range of operating conditions, such as significant temperature and pressure fluctuations, and environmental changes. Furthermore, the use of a simple TiN matrix often fails to improve wear resistance. As noted in [5], the use of a TiN coating failed to improve the wear resistance of Q&T SAE 4140 steel, while the use of ion nitriding as single surface treatment reduced the surface wear rate.

There are numerous approaches to improving the performance of solid lubricant coatings. Formation of nanostructured, nanocomposite, or multilayer coatings using ion-plasma technologies can improve the properties of solid lubricant coatings and coatings for other applications [10–15].

The formation of a composite SLC by adding soft, "easily sheared" metals that do not form stable nitrides, such as Ag [16], Cu [17, 18], In [19], and Pb [20–22], to a nitride coating can reduce the friction coefficient and increase wear resistance. In these studies, it was found that the addition of these metals leads to a weakening of the pronounced texture of TiN coatings obtained by magnetron sputtering, resulting in a decrease in the friction coefficient. The addition of soft metals with a low tendency to nitridation to the TiN coating composition is in many cases accompanied by grain refinement to nanoscale, which contributes to an increase in microhardness and improvement of tribological characteristics. Thus, in work [23], a friction coefficient of ~0.08 at a temperature of 900 °C was obtained for VN/Ag nanocomposite films. Another approach to improving coating performance is an application of ternary nitride coatings based on transition metals such as TiSiN, TiAlN, and TiZrN [3,10]. An alloying with Zr or V improves the wear resistance of TiN coatings by shifting the dominant wear mechanism from adhesive to abrasive in tests where an AISI 52100 steel ball was used as a counter body as was shown in work [24].

The formation of a multicomponent composite matrix or one with the properties of medium- or high-entropy ceramics can significantly improve such coating characteris-

tics as hardness, thermal and chemical stability, and wear resistance. In work [25] the deposition of a multicomponent Ti–TiN–(Ti, Nb, Zr, Al)N coating was produced by filtered cathodic vacuum-arc deposition on AISI-1045 steel. It was observed an increase in tool life by more than three times compared to untreated steel. In [26], the production of AlCrTiV–N and AlCrTiVS–N coatings by magnetron sputtering and subsequent nitriding on 304 steel improved the tribological properties. The AlCrTiV–N film had a friction coefficient of ~ 0.2 and the best wear resistance. Magnetron sputtering was used to obtain high-entropy nitride coatings (AlCrNbSiTiMo)N using a bias voltage of both substrates and at a deposition temperature of 300 °C [27]. The coatings have a hardness of 34.5±0.8 GPa. The coatings obtained at a bias voltage of –100 V and tested for wear at a film temperature of 700 °C, showed the lowest wear rate of about 1.2×10^{-6} mm^3 per 1 m^{-1} and a friction coefficient of 0.48. In [28], high-entropy TiAlNiVN coatings were deposited by magnetron sputtering on D2 tool steel with the hardness reached 25.7 GPa, and the wear rate was 2.45×10^{-5} mm^3/(N·m) with a friction coefficient of 0.44. High-entropy nitride films were also studied in articles [29–30]. In [31], the positive influence of the average entropy structure of TiAlZrN coatings with In and Sn additives and without additives on tribological and mechanical characteristics was shown.

Another approach to improving the performance of solid lubricant coatings is the use of the tribooxidation. In this case, the solid lubricant coating itself acts as a source of elements for tribochemical oxidation reactions, resulting in the formation of lamellar oxides and oxynitride phases on their surface, acting as a high-temperature lubricant [23, 32–33].

This work is aimed at research of the soft metals – indium (1.4–5.7 at. %) and tin (0.1–0.7 at. %) content effect in TiAlZrN based hard matrix coatings deposited on AISI 304 steel, on the surface morphology, structure and tribological characteristics at room and elevated temperatures under fretting wear conditions in contact with a counterbody made of ShKh-15 steel.

Experimental part

TiAlZrN-InSn coatings were obtained by reactive magnetron sputtering of separate cathodes (titanium VT1-0), aluminum (99.9 %), zirconium (99.5 %), InSn (80 % In, 20 % Sn) on 1 samples of AISI 304 steel (Ni 8.63 %, Cr 16.04 %, C 0.047 %, Si 0.48 %, Mn 1.37 %, S 0.005 %, Mo 0.09 %, and P 0.029 % wt.). The size and the thickness of the samples were 15 × 15 mm and 1 mm. The distance from the magnetrons to the samples was 125 mm, and the distance from the ion source to the samples was 170 mm. The screens made of 304 steel were situated near them to reduce the possible transfer of sputtered atoms from one magnetron to another. Ar and N gases were supplied to the vacuum chamber through an ion source. The steel samples were cleaned in an ultrasonic bath in gasoline for 10–15 min before deposition. The pressure in the chamber reached $6.0 \cdot 10^{-4}$ Pa. Primarily, the surface of the samples was cleaned in a glow discharge for 15 minutes. Then, the pumping was carried out up $P_{Ar} = 6.0 \cdot 10^{-4}$ Pa with liquid nitrogen, and Ar was injected up $P_{Ar} = 5.3 \cdot 10^{-2}$ Pa (Ar flow rate – 2.55 cm^3/min) and the substrate was cleaned with the ion source turned on for 20 min. while rotating.

Transition layers of Ti (5 min) and TiN (5 min) were formed before the main layer deposition. The main layer of TiAlZrN–InSn was formed for 50 min at substrate rotated with a speed of 2 rpm. The clockwise rotating substrate sequentially entered the sputtering areas of Ti, Zr, Al, and InSn targets. The main parameters of the coatings deposition modes are presented in **Table 1**. A mid-frequency mode (50 kHz) was used for Ti, Al, Zr, and InSn deposition. For coatings 2 and 7, titanium, aluminum, and zirconium were sputtered at fill factors of 80 %, while for sample 1, the fill factors were 60 %, 30 %, and 30 %. The fill factor of InSn sputtering was 30 % for samples 1–3, and 80 % for other samples. Coatings 5–7 were deposited with the ion source operating. The average coating thickness was 1 μm.

The morphology and composition of the coatings were analyzed using a Carl Zeiss Evo scanning electron microscope equipped with energy-dispersive X-ray analysis (EDX). Surface roughness and volumetric imaging were analyzed using an Olympus LEXT OLS confocal microscope. The surface roughness of the coating was assessed in accordance with ISO 25178—2:2012. X-ray diffraction analysis (XRD) was carried out using a DRON-7 X-ray diffractometer using filtered CuK_α radiation with a wavelength of $\lambda_{av} = 1.54178$ Å. The microhardness of the coatings was analyzed using a PMT-3 instrument by indenting a Vickers pyramid with a 50 g load.

Tribological tests using a sphere-on-disk scheme were conducted in fretting wear simulating mode with a displacement of 15 μm. A 12.6 mm diameter sphere made of ShKh-15 steel (C 0.95 %, Cr 1.3 %, Si 0.17 %, Mn 0.4 %, Ni <0.3 %, Cu<0.25 %, S<0.02 %, the rest is Fe) with a hardness of up to 65 HRC was used as the counterbody. Tests were carried out at an ambient temperature of 23 °C and a humidity of 37±5 %. The normal contact load was 1 N,

Table 1. Deposition parameters. Q_{Ar}, Q_{N2} – gas flow rates; I_{Ti}, I_{Al}, I_{Zr}, I_{InSn} – discharge currents; IS-ion source

Coating	P_{Ar+N2}, Pa	P_{N2}, Pa	Q_{Ar}, cm^3/min	Q_{N2}, cm^3/min	I_{Ti}, A	I_{Al}, A	I_{Zr}, A	I_{InSn}, A	I_S
1	0.33	$2.4 \cdot 10^{-2}$	8.55	1.7	6	1	1	0.3	off
2	0.40	$2.3 \cdot 10^{-2}$	9.71	1.72	6	1	2	0.3	off
3	0.40	$2.3 \cdot 10^{-2}$	9.55	1.61	6	1.5	2	0.2	off
4	0.40	$2.3 \cdot 10^{-2}$	9.62	1.61	6	1.5	2	0.5	off
5	0.40	$2.3 \cdot 10^{-2}$	9.80	1.61	6	1	2	0.5	on
6	0.40	$2.3 \cdot 10^{-2}$	9.74	1.63	6	1.3	2	0.5	on
7	0.40	$4.0 \cdot 10^{-1}$	9.74	1.63	6	1.5	2	0.5	on

and the displacement frequency was 20 Hz, the number of cycles was 50000. Wear scars were examined using an Olympus LEXT OLS confocal microscope to assess volumetric wear. Tribological tests after stepwise heating in a muffle furnace to temperatures of 100 and 200 °C and holding at each temperature for 2 hours were carried out for 10000 cycles using identical loading parameters.

Results and Discussion

Coating Structure, Composition, and Roughness

The elemental composition of the coatings according to EDX data is shown in **Fig. 1**. Indium content varied from 1.4 to 5.7 at. %, and tin content from 0.1 to 0.8 at. %. The initial roughness (Ra) of steel substrates was 0.05 μm, and it varied from 0.03 to 0.5 μm after coating deposition. Micrometer-scale protrusions are also present on the surface of the smoothest coatings. Their presence should undoubtedly influence the tribological characteristics of the steel substrate–coating system, especially during the initial test cycles.

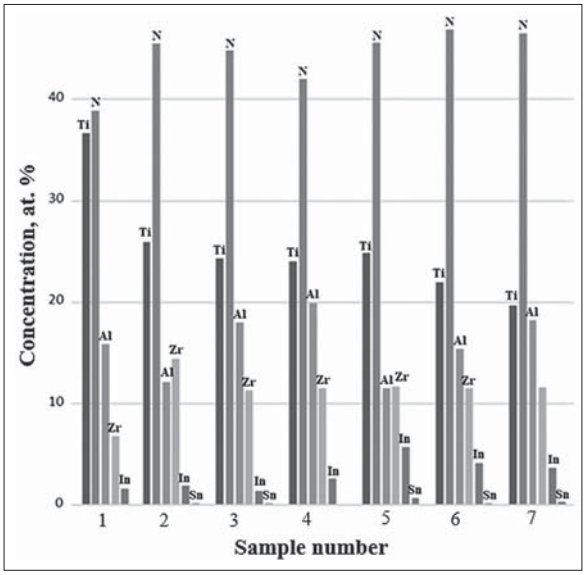

Fig. 1. Composition of the coatings according to EDX data

The surface structure of the coatings significantly changed from smooth to coarse-globular with an increase in the indium content from 1.4 to 5.7 at. % (**Fig. 2**). The surface of the coating 3 with an indium content of approximately 1.4 at. % was smooth and uniform. The roughness of the steel substrate with this film decreased (Ra = 0.03 μm) (Fig. 2, *a*). At an indium content of 1.6 at. %, the structure was finely crystalline. The tracks after mechanical treatment of the steel are visible, and the Ra parameter is 0.04 μm (Fig. 2, *b*). The indium content increased to 1.9 % in coating 2, the film became nanocrystalline, but the roughness remains low at Ra = 0.03 μm (Fig. 2, *c*). Moreover,

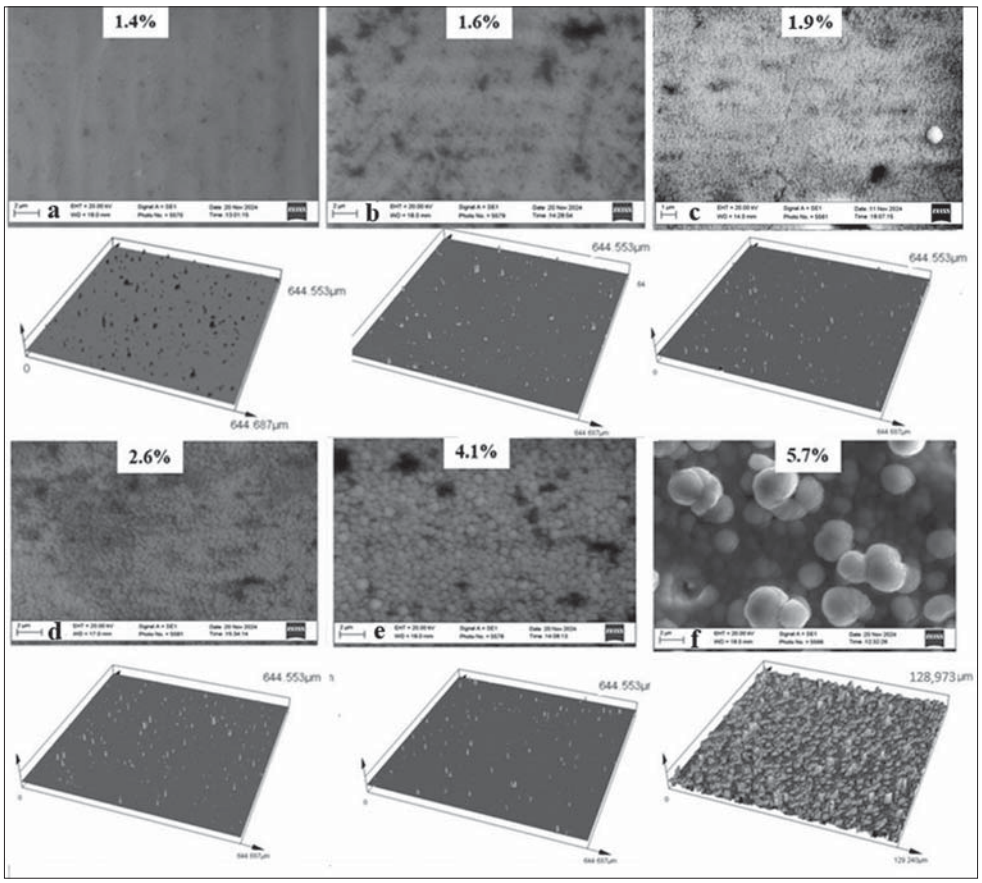

Fig. 2. SEM images in secondary electrons of the coating surface with different indium content: 3 (*a*), 1 (*b*), 2 (*c*), 4 (*d*), 6 (*e*), 5 (*f*) and 3D visualization patterns of the surfaces obtained by confocal microscope

three-dimensional visualization of the surface shows an approximately identical packing density of micrometer-scale protrusions on the surface for all three coatings (1–3). Increasing in the indium content to 2.6 at. % in coating 4 resulted in some increase in the globule size, but the roughness did not change significantly, Ra = 0.04 μm (Fig. 2, *d*). The sample with coating 7 (In 3.7 at. %) was characterized the globule size increased to 0.4 μm, and the roughness Ra = 0.07 μm. Increasing the indium content in the coating 6 to 4.1 at. % resulted in an increase in the average globule size (~0.7 μm), and Ra to 0.1 μm (Fig. 2, *e*). Deposition mode 5 resulted in an increase in the indium content to 5.7 at. % in the coating. The surface became more developed with pronounced globularity. The globule size reached 3 μm, and Ra increased to 0.9 μm (Fig. 2, *f*).

Three-dimensional surface visualization images show that the density of microroughnesses is approximately the same for samples with an indium content of up to 4.1 %. However, with a further increase in its content, the surface development significantly increases, becoming globular. The globularity of the coatings, in addition to the content of soft metals, could be influenced by the ratio of other elements, as suggested in work [31]. Thus, it was found that with an indium content of 5.1 at. %, the coating structure was looser, and the roughness Ra was 1.2 μm, which is higher than with an indium content of 5.7 at. % in this work (Ra = 0.9 μm). The formation of a globular surface of the deposited coating can be caused by the presence of compressive stresses in the surface layer [34].

The surface "globularity" was absent for the coatings without InSn addition. The coating roughness corresponded to the initial substrate roughness. With increasing InSn content in the coatings, its phase migration into the surface layer could occur, leading to an increase in thermal stresses, as was found for TiN–Cu coatings in work [17].

Roughness analysis showed that a decrease in the roughness parameters Ra and Rq was generally not accompanied by a decrease in the parameter Rz, i.e., coatings with a sufficiently smooth surface still retained relatively high surface protrusions. Rz parameter did not differ significantly between the coating with the most developed surface (5) and the smoother coatings. However, Rz was significantly lower for coatings without indium, suggesting a significant influence on surface development due to its phase migration, which contributed to stress in the surface layer.

Coating Phase Composition

Fig. 3 shows XRD patterns of coatings with indium content of 1.6, 2.6, 4.1, and 5.7 at. % and tin content of 0.1, 0.1, 0.2, and 0.7 at. %. All patterns show reflections from the steel substrate with an FCC lattice and reflections from nitride phases with a NaCl-type lattice.

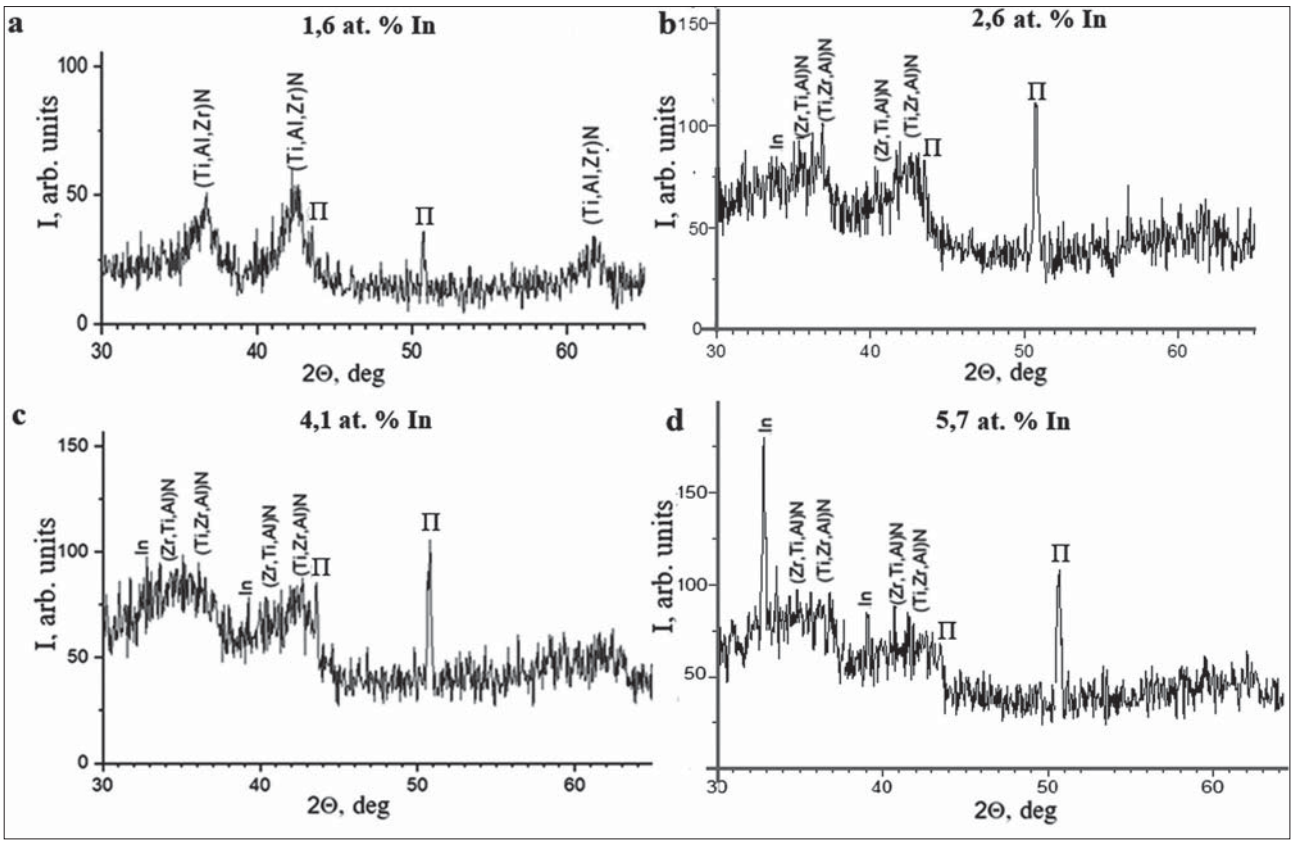

Fig. 3. XRD patterns of coatings 1 (*a*), **4** (*b*), **6** (*c*), **5** (*d*)

A weak indium reflection (In(Sn) solid solution) appears at an indium content of 2.6 at. % in XRD pattern at 2θ = 33° for coating 4 with a two-phase nitride structure of (Ti,Al,Zr)N and (Zr,Ti,Al)N (Fig. 3, *b*). There are not indium reflections in patterns of coating 3 (1.4 at. % In) and coating 1 with an indium content of 1.6 at. % and a single-phase nitride structure (Fig. 3, *a*), as well as for coating 2 with a two-phase nitride structure and an indium content of 1.9 at. %. In (Sn) reflections are visible in the XRD patterns of two-phase nitride coatings 7 with an indium content of 3.7 at. % and coating 6 with an indium content of 4.1 at. % in the region of reflection angles 2θ = 33 and 39° (Fig. 3, *c*). The intensity of indium reflections significantly increases with an increase in its content to 5.7 at. % for two-phase nitride coating 5 (Fig. 3, *d*).

Tribological Characteristics and Microhardness

Stable friction coefficient values of ~0.20 were demonstrated for coatings 2 (In 1.9 at. %), 3 (In 1.4 at. %), and 7 (In 3.7 at. %) in the contact with a ShKh-15 steel sphere throughout the entire test cycle (**Fig. 4,** *a*). These coatings also exhibited the lowest volumetric wear (Fig. 4, *b*). The friction coefficient of coating 4 (In 2.6 at. %) was ~0.24, and fluctuations are visible in the graphs, which may be related to the accumulation of wear debris in the contact zone and its removal beyond the contact patch. The friction coefficient of coating 6 (In 4.1 at. %) gradually increased to 0.27 during testing, while for coating 1 (In 1.6 at. %), it remained approximately 0.30 throughout the entire test cycle. The highest friction coefficient was obtained on the sample with coating 5 (~0.42) with the highest In content (5.7 at. %). At the same time, many coatings exhibited counter body material transfer, appeared in increased wear patch height relative to the coating surface ("positive wear"). It is the greatest for coatings 4, 5, and 7. Moreover, the graphs of the friction coefficient dependences did not show any significant changes for 50000 test cycles. Mass transfer may be related to chemical interaction between the samples and the counter body, occurring during the first 3,000 cycles. It may be appeared as a sharp increase in the friction coefficient, followed by a decrease and attainment of a constant value, which is most noticeable for samples 3, 4, 5, and 7.

Negative volumetric wear is caused mainly by abrasion, and positive wear is due to the adhesive mechanism (sticking). Thus, abrasive and adhesive wear mechanisms predominated for the coatings. For some coatings, the applied load led to chemical interaction due to heat in the contact zone as a result of friction. At the initial stage, the interaction mainly occurred via the abrasive wear mechanism, arising from the contact of hard microroughnesses of the nitride coating surface and their movement along the counter body surface. Then they smoothed out, which is shown by a sharp

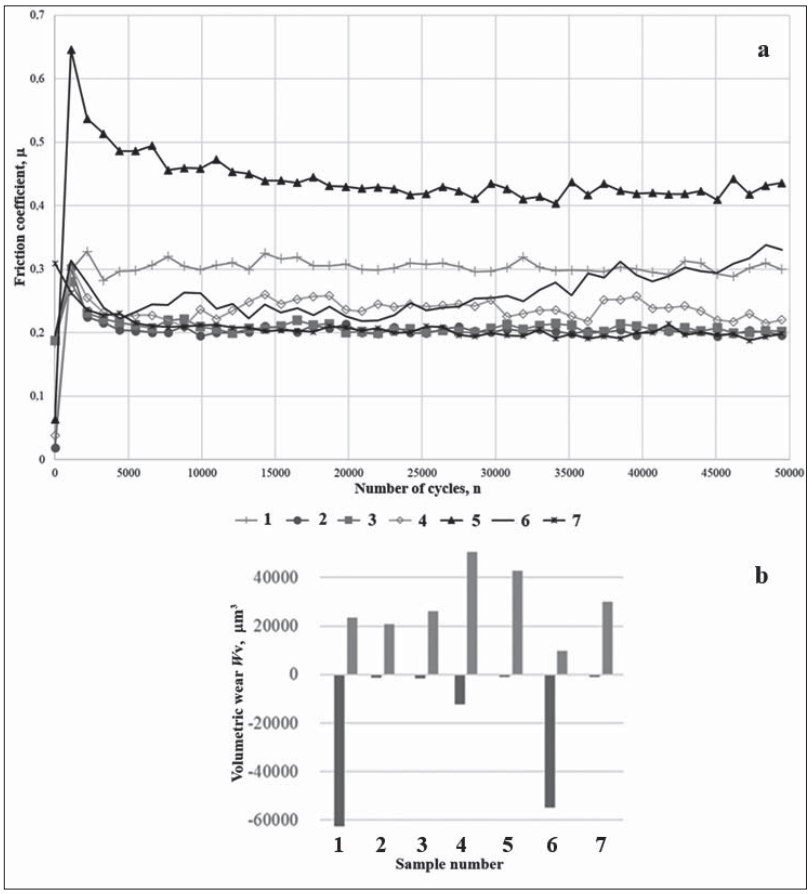

Fig. 4. Graphs of changes in the friction coefficient of coatings depending on the test cycle (*a*), and the values of volumetric wear W_{v-} and material adhesion W_{v+} (*b*)

rise and fall in the friction coefficient graphs. Depending on the coating structure, further wear occurred via the abrasive mechanism with the separation of hard particles of the nitride matrix. In other cases, further wear continued via the adhesive mechanism: due to micro welding of roughnesses; due to chemical interaction of the coating material and the counter body for coatings with a high content of soft metals; during partial destruction of the coating during interaction with the substrate. This wear mechanism is classified as fretting wear, as the products of interaction remain in the contact zone, and the friction coefficient remains unchanged over a large number of cycles. With further dissipation of thermal energy in the contact zone and interaction with the environment, the structure of the resulting "third body" may change: the content of oxides and oxynitrides increases, which can reduce friction and wear, and an iron-rich transferred layer may form on the coating surface, protecting the coating from further abrasion.

SEM studies have shown the presence of micro hills on the surface of the coatings, in some cases exceeding the film thickness in magnitude. In work [34], it is indicated that such structural features grow in films of materials with a low melting point under conditions of high compressive stress. The resulting coatings have a combined structure containing a hard matrix and additional soft phases, which can lead simultaneously to both tensile internal stresses arising during the growth of columnar crystallites and compressive stresses, for example, in the surface layer, leading to the appearance of high micro hills. In the case of the hard coatings, such particles can cause more intense abrasive wear, since their exit from the contact zone is difficult during fretting wear. The number of abrasive particles can increase during grinding for globular coatings. Therefore, the stability of tribological characteristics was demonstrated, including by coatings with not the highest hardness, for example, 3. During the wear process the microroughnesses were ground down and did not cause further destruction.

The microhardness of AISI 304 steel with the coatings varied from 2.9 to 10.3 GPa (**Table 2**). The highest microhardness was obtained for coating 1 with an indium content of 1.6 at. % and a single-phase nitride structure. An increase in the indium content led to a decrease in microhardness. Thus, it decreased to 2.9 GPa for coating 5 (In 5.7 at. %). However, the coating hardness was influenced not only by the indium content, but also by the ratio of other elements, as well as the structure type. Thus, for coating 4 (In 2.6 at. %) with a two-phase nitride structure and the In(Sn) phase presence in the XRD pattern, the microhardness decreased to 7.3 GPa, and for coating 7 (In 3.7 at. %) it increased to 8.0 GPa. The coatings with a large-globular surface structure demonstrated the lowest hardness values.

Tribological Characteristics after Stepwise Heating

Tribological tests using stepwise heating were conducted for substrates with coatings 2 (In 1.9 ат. %, Sn 0.2 ат. %), 3 (In 1.4 ат. %, Sn 0.1 ат. %) and 7 (In 3.7 ат. %, Sn 0.3 ат. %), which demonstrated the lowest friction coefficients at room temperature. Increased softening at high temperatures can lead to the soft component being drawn out from the interface, limiting its lubricating effect. On the other hand, lamellar oxides and oxynitride phases can form on the coating surface, acting as a high-temperature lubricant.

Coating 2 demonstrated the greatest stability in tribological characteristics after heating to both 100 °C and 200 °C (**Fig. 5**). As a result of heating to 100°C, the friction coefficient decreases to 0.1 (from 0.20 at room temperature), and to 0.08 at 200 °C (Fig. 5, *b*). The wear patch is almost absent in the confocal microscopy image (**Fig. 6**, *a*).

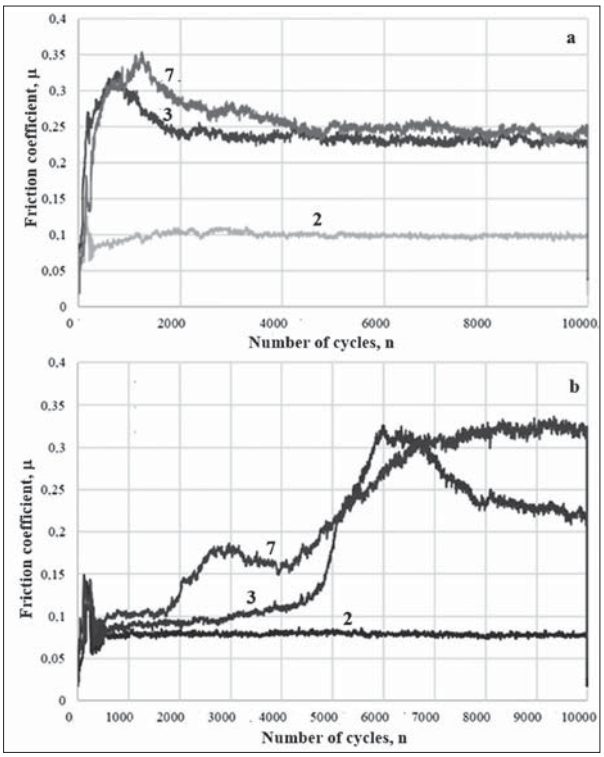

Fig. 5. Friction coefficients of the coatings 2 (1,9 at. % In), 3 (1,4 at. % In), and 7 (3.7 at. % In) as a result of heating to 100 °C (*a*) and 200 °C (*b*)

Table 2. Volumetric wear, wear patch depth, friction coefficients μ, Vickers microhardness, and indium content in the coatings

No.	Wear volume, μm³	Wear patch depth, μm	Friction coefficient, μ	$HV_{0.05}$, GPa	In, at. %
1	62582	2.537	0.30	10.3	1.6
2	1356	0	0.20	9.9	1.9
3	1390	0	0.21	7.5	1.4
4	12169	1.968	0.24	7.3	2.6
5	814	0	0.42	2.9	5.7
6	54882	2.751	0.27	6.3	4.1
7	1057	0	0.20	8.0	3.7

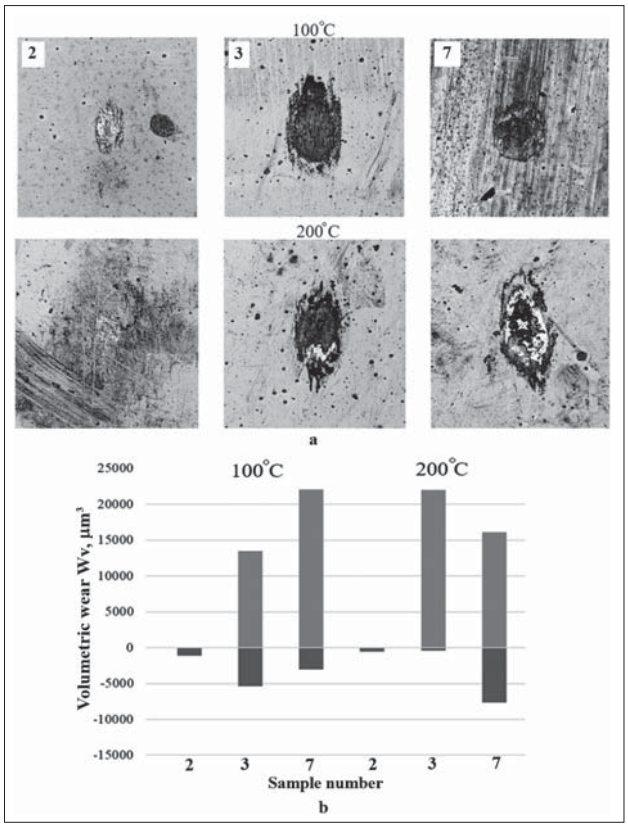

Fig. 6. Wear patch images after heating to 100 °C and 200 °C for samples with coatings 2 (1,9 at. % In), 3 (1,4 at. % In) and 7 (3.7 at. % In) (*a*), and comparison of the volumetric wear (W_{v-}) and the amount of material transferred (W_{v+}) after heating samples to 100 °C and 200 °C (*b*)

Upon heating to 100 °C, samples 3 and 7 showed a similar trend in friction coefficient change. Primary, it was a sharp increase, possibly due to material transfer from the counter body, followed by the grinding process and a decrease in the coefficient to 0.23 (Fig. 5, *a*). However, it was slightly higher than that observed at room temperature. The wear patch is less pronounced for coating 7 (Fig. 6, *a*). Heating to 200 °C resulted in more significant fluctuations in the friction coefficient graphs. There were initial increase and then a drop to approximately 0.22 for coating 3, and an increase to 0.32 for coating 7.

Wear decreased with increasing test temperature, and no material transfer from the counter body was observed for coating 2 (Fig. 6, *b*).

Stepwise heating increased wear, but decreased counter body material transfer of coating 7. Both, negative and positive wear decreased for coating 3 (Fig. 6, *b*). This different behavior of the coatings is due to their structure. There is a two-phase nitride structure with an indium content of 1.4–1.9 at. % in coatings 2 and 3. Coating 7 has a three-phase structure with an indium content of approximately 3.7 at. %. The low melting point of indium could have caused this change in the coating properties after heating to 200 °C.

The coatings had to be subjected to oxidation during heating, which affected their tribological properties. Some improvement/change in these properties could have been due to the formation of oxides and oxynitrides of the system components. Oxygen atoms can be incorporated into the Ti–Al–Zr–N nitride matrix, forming a complex oxynitride that retains the original crystalline structure (such as NaCl). In this case, oxygen atoms replace some of the nitrogen atoms without forming oxides [24, 35].

As can be seen from the wear patch images and volumetric wear characteristics, abrasive and adhesive mechanisms predominate. Dark areas in the wear patch images correspond to material "transferred" from the counter body. In the absence of an adhesion mechanism, the wear scar is light-colored, as obtained for coating 2 (fig. 6, *a*). The oxide layer formed as a result of stepwise heating is destroyed by friction under the effect of load, which can lead to the formation of small abrasive particles. They can adhere to the contact surface and are compressed under the effect of force, forming a transition layer. In addition, small particles can appear as a result of the destruction of micron-sized hills on the surface, detected by confocal microscopy. These particles adhere to the wear surface and agglomerate in some areas, mainly in the valleys [36]. Oxide particles can also be trapped in the gaps between the sliding surfaces, forming a protective layer [24]. Thus, as a result of heating, the wear mechanisms are mainly associated with adhesion, abrasion, and diffusion processes. Black spots indicate deformed residues formed under the influence of high temperature and adhesion, explaining the cyclic changes in the friction coefficient. The wear patches also have a shear relief along the direction of the counterbody's movement, which is due to the presence of soft metals in the coatings. The soft components of the coating plastically deformed during sliding, reducing friction and wear. Coating 2, with a two-phase nitride fine-crystalline structure and a low indium content, has demonstrated more stable properties. XRD data showed that indium was absent as a separate phase in this coating.

Conclusion

1. Coatings based on the complex TiAlZrN matrix with an indium content of 1.4 – 5.7 at. % and tin content of 0.1 – 0.8 at. % were obtained on AISI 304 steel by reactive magnetron sputtering of separate cathodes (titanium grade VT1-0, aluminum (99.9 %), zirconium (99.5 %), InSn (80 % In, 20 % Sn). Reflexes of the In(Sn) solid solution appear on XRD patterns when indium content in the coatings is more than 2.6 at. %.

2. The surface structure of the coatings changed from smooth to finely crystalline with an increase in the indium content from 1.6 to 1.9 at. %, and to microglobular with an increase in the indium content to 5.7 at. %, which was also accompanied by an increase in surface roughness. A decrease in the roughness parameters Ra and Rq was generally not accompanied by a decrease in the Rz parameter. The coatings with a sufficiently smooth surface had individual micro hills on the surface.

3. The friction coefficients at room temperature varied from 0.20 to 0.42. Abrasive and adhesive wear mechanisms predominated for the coatings. Heating to 100 °C resulted in a decrease in the friction coefficient to 0.10 for the coating with an indium content of 1.9 at. %, and to 0.08 after heating up 200 °C, which was also accompanied by a decrease in wear.

4. The presence of a nanocrystalline structure and the absence of indium as a separate phase contributed more to stable tribological characteristics at room temperature and after stepwise heating than a denser, homogeneous coating structure with a lower indium content or a globular structure.

The work was carried out with the support of the Ministry of Education and Science of Russia, Grant No. FSFF-2023-0006

REFERENCES

1. Saetang V., Taweejun N., Zhu H., Jaafar H., Daodon W. Effects of laser texturing on tribological properties and wettability of titanium nitride-coated AISI M2 high-speed steel. *Surface & Coatings Technology*. 2024. Vol. 490. 131173.
2. Neto J. F. M., Naeem M., Lima L. F., Yang Y., Liborio M. S., Feitor M. S., Alves S. M., Sousa R. R. M., Iqbal J., Costa T. H. C., Nascimento R. M. Improved wear resistance of AISI-4340 steel by Ti–Nb–C–N and MoS_2 composite coating by cathodic cage plasma deposition. *Physica B: Condensed Matter*. 2024. Vol. 676. 415652.
3. Alves U. C., Ricci V. P., Mota I. G. C., Koga G., Hassui A., Ventura C. E. H. Mechanical and tribological characterization of TiAlN/TiN and TiSiN/AlTiN coating systems for cutting tools. *Journal of Manufacturing Processes*. 2025. Vol. 145. pp. 522–535.
4. Vales S., Avila P. R. T., Rosenkranz A., Droppa Jr. R., Soldera F., Garcia J., Alvarez F., Pinto H. Effect of ion peening and pulsed plasma nitriding on the structural properties of TiN coatings sputtered onto 100Cr6 steel. *Materials Chemistry and Physics*. 2019. Vol. 235. pp. 121723–121731.
5. Mandri A. D., Colombo D. A., Sanchez N. V., Brühl S. P., Dommarco R. C. Rolling contact fatigue of ion nitrided and TiN coated AISI 4140 steel under pure rolling condition. *Engineering Failure Analysis*. 2025. Vol. 170. 109311.
6. Hacisalihoglu I., Yildiz F., Alsaran A. Wear performance of different nitride-based coatings on plasma nitrided AISI M2 tool steel in dry and lubricated conditions. *Wear*. 2017. Vol. 384–385. pp. 159–168.
7. Feng W., Yan D., He J., Li X., Dong Y. Reactive plasma sprayed TiN coating and its tribological properties. *Wear*. 2005. Vol. 258. No. 5–6. pp. 806–811.
8. Vereschaka A., Grigoriev S., Tabakov V., Migranov M., Sitnikov N., Milovich F., et al. Influence of the nanostructure of Ti–TiN–(Ti,Al,Cr)N multilayer composite coating on tribological properties and cutting tool life. *Tribology International*. 2020. Vol. 150. 106388.
9. Smyrnova K., Sahul M., Haršáni M., Pogrebnjak A., Ivashchenko V., Beresnev V., et al. Microstructure, mechanical and tribological properties of advanced layered WN/MeN (Me=Zr, Cr, Mo, Nb) nanocomposite coatings. *Nanomaterials*. 2022. Vol. 12. No. 3. 395.
10. Maksakova O. V., Zhanyssov S., Plotnikov S., Konarski P., Budzynski P., Pogrebnjak A. et al. Microstructure and tribomechanical properties of multilayer TiZrN/TiSiN composite coatings with nanoscale architecture by cathodic-arc evaporation. *Journal of Materials Science*. 2021. Vol. 56. pp. 5067–5081.
11. Polyanskii M. N., Savushkina S. V. Lateral layer-by-layer nanostructuring of thermal barrier coatings of zirconium dioxide during plasma spraying. *Journal of Surface Investigation. X-ray, Synchrotron and Neutron Techniques*. 2014. Vol. 8. No. 1. pp. 144–148.
12. Zhang L., Shen Y.-Q., Zhao Y.-M., Chen S.-N., Ouyang X., Zhang X., et al. Structure control of high-quality TiAlN monolithic and TiAlN/TiAl multilayer coatings based on filtered cathodic vacuum arc technique. *Surfaces and Interfaces*. 2023 Vol. 38. 102836.
13. Aouadi S. M., Singh D. P., Stone D., Polychronopoulou K., Nahif F., Rebholz C., Muratore C., Voevodin A. A. Adaptive VN/Ag nanocomposite coatings with lubricious behavior from 25 to 1000 °C. *Acta Materialia*. 2010. Vol. 58. No. 16. pp. 5326–5331.
14. Wang Z., Li X., Wang X., Cai S., Ke P., Wang A. Hard yet tough V–Al–C–N nanocomposite coatings: microstructure, mechanical and tribological properties. *Surface and Coatings Technology*. 2016. Vol. 304. pp. 553–559.
15. Zaitsev A. N. Antifriction characteristics of the magnetron sputtered MoS2 coating of ITER blanket module bolted joints in high vacuum at elevated temperature T = 250 °C. *Vacuum*. 2024. Vol. 230. Part A. 113615.
16. Liu C., Gu X., Yang L., Song X., Wen M., Wang J., Li Q., Zhang K., Zheng W., Chen C. Ultralow-friction and ultralow-wear TiN–Ag solid solution coating in base oil. *The Journal of Physical Chemistry Letters*. 2020. Vol. 11. No. 5. pp. 1614–1621.
17. Blinkov I. V., Volkhonskii A.O., Laptev A.I., et al. Ceramic-metallic (TiN–Cu) nanostructured ion-plasma vacuum-arc coatings for cutting hard-alloy tools. *Russian Journal of Non-Ferrous Metals*. 2014. Vol. 55. No. 5, pp. 489–493.
18. Ye F., Sun X. Nanoindentation response analysis of TiN–Cu coating deposited by magnetron sputtering. *Progress in Natural Science: Materials International*. 2018. Vol. 28. No. 1. pp. 40–44.
19. Guleryuz C. G., Krzanowski J. E., Veldhuis S. C., Fox-Rabinovich G. S. Machining performance of TiN coatings incorporating indium as a solid lubricant as placeholders for microreservoir formation. *Surface and Coatings Technology*. 2009. Vol. 203. No. 20–21. pp. 3370–3376.
20. Lozovan A. A., Betsofen S. Y., Savushkina S. V., Lychovetsky M. A., Lesnevsky L. N., Nikolaev I. A., Kubatina E. P. Influence of sputtering geometry and conditions on the structure and properties of the TiN–Pb solid lubricating coatings fabricated by magnetron co-sputtering of two separate targets. *Russian Metallurgy (Metally)*. 2022. No. 11. pp. 1441–1448.
21. Lesnevskii L. N., Tyurin V. N., Ushakov A. M. Method for formation of composite solid-lubricating coatings on working surfaces of frictional units. Patent 2416675 RF. 20.04.2011.
22. Lozovan A., Savushkina S., Lyakhovetsky M., Nikolaev I., Betsofen S., Kubatina E. Investigation of Structural and Tribological Characteristics of TiN Composite Ceramic Coatings with Pb Additives. *Coatings*. 2023. Vol. 13. No. 8. 1463.
23. Guo H., Lu C., Zhang Z., et al. Comparison of microstructures and properties of VN and VN/Ag nanocomposite films fabricated by pulsed laser deposition. *Applied Physics A*. 2018. Vol. 124. 694.
24. Kumar A., Mulik R. S. Improving tribological behavior of titanium nitride (TiN) hard coatings via zirconium (Zr) or vanadium (V) doping. *Tribology International*. 2023. Vol. 189. 108997.
25. Grigoriev S. et al. Investigation of the properties of Ti–TiN–(Ti, Al, Nb, Zr)N composite coating and its efficiency in increasing wear resistance of metal cutting tools. *Surface and Coatings Technology*. 2021. Vol. 421. 127432.
26. Cai Z., Wang Z., Hong Y., Lu B., Liu J., Li Y., Pu J. Improved Tribological Behavior of Plasma-Nitrided AlCrTiV and AlCrTiVSi High-Entropy Alloy Films. *Tribology International*. 2021. Vol. 163. 107195.
27. Lo W.-L., Hsu S.-Y., Lin Y.-C., Tsai S.-Y., Lai Y.-T., Duh J.-G. Improvement of High Entropy Alloy Nitride Coatings (AlCrNbSiTiMo)N on Mechanical and High Temperature Tribological Properties by Tuning Substrate Bias. *Surface and Coatings Technology*. 2020. Vol. 401. 126247.
28. Yılmaz A. M., Çiçek H., Duran S., Gülten G., Efeoğlu İ. Investigation of hardness, tribological and adhesion properties of TiAlNiVN HEA films heat treated at different temperatures. *Tribology International*. 2024. Vol. 197. 109739.
29. von Fieandt K., Paschalidou E.M., Srinath A., Soucek P., Riekehr L., Nyholm L., et al. Multi-component (Al,Cr,Nb,Y,Zr)N thin films by reactive magnetron sputter deposition for increased hardness and corrosion resistance. *Thin Solid Films*. 2020. Vol. 693. 137685.
30. Hsieh M. H., Tsai M. H., Shen W. J., Yeh J. W. Structure and properties of two Al–Cr–Nb–Si–Ti high-entropy nitride coatings. *Surface and Coatings Technology*. 2013. Vol. 221. pp. 118–123.
31. Lozovan A. A., Betzofen S. Ya., Savushkina S. V., Nikolaev I. A., Zhukov E. Yu., Babaitsev A. V. Structure and tribological characteristics of TiAlZrN–InSn system based coatings. *Metals*. 2025. No. 1. pp. 20–29.
32. Cai Q., Bai X., Pu J. Adaptive VAlCN-Ag composite and VAlCN/VN–Ag multilayer coatings intended for applications at elevated temperature. *Journal of Materials Science*. 2022. Vol. 57. pp. 8113–8126.
33. Gudala S., Ramesh M. R., Nallathambi S. S. Evolution of Microstructure and High-Temperature Tribological Performance of Self-Lubricating Nickel-Based Composite Tungsten Inert Gas Coatings. *Journal of Materials Engineering and Performance*. 2021. Vol. 30. pp. 8080–8094.
34. Thornton J. A., Hoffman D. W. Stress-related effects in thin films. *Thin Solid Films*. 1989. Vol. 171. No. 1. pp. 5–31.
35. Suciu C. V., Uchida T. Modeling and Simulation of the Fretting Hysteresis Loop. *Proceedings of the 3PGCIC 2010, International Conference on P2P*. Fukuoka, Japan, 2010. p. 560.
36. Pettersson M., Skjoldebrand C., Filho L., Engqvist H., Persson C. Morphology and dissolution rate of wear debris from silicon nitride coatings. *ACS Biomaterials Science & Engineering*. 2016. Vol. 2. No. 6. pp. 998–1004.